INTERNATIONAL JOURNAL OF CLIMATOLOGY
Int. J. Climatol. **36**: 2173–2188 (2016)
Published online 14 September 2015 in Wiley Online Library
(wileyonlinelibrary.com) DOI: 10.1002/joc.4485

RMetS
Royal Meteorological Society

Climatology and trend of wind power resources in China and its surrounding regions: a revisit using Climate Forecast System Reanalysis data

Lejiang Yu,[a,b] Shiyuan Zhong,[b]* Xindi Bian[c] and Warren E. Heilman[c]

[a] *Applied Hydrometeorological Research Institute, Nanjing University of Information Science & Technology, China*
[b] *Department of Geography and Center for Global Change and Earth Observations, Michigan State University, East Lansing, MI, USA*
[c] *Northern Research Station, USDA Forest Service, Lansing, MI, USA*

ABSTRACT: The mean climatology, seasonal and interannual variability and trend of wind speeds at the hub height (80 m) of modern wind turbines over China and its surrounding regions are revisited using 33-year (1979–2011) wind data from the Climate Forecast System Reanalysis (CFSR) that has many improvements including higher spatial resolution over previous global reanalysis products. Mean 80-m wind speeds are consistently higher over China Seas and the ocean areas than over land, and inside China high winds are found in areas of Inner Mongolia and the Tibetan Plateau. There is a considerable seasonal variability that reflects primarily the influence of East and Southeast Asia Monsoon with generally higher speeds in winter followed by summer, and weaker winds in autumn, followed by spring. There is also a strong interannual variability, and regions of larger amplitude of variability coincide with regions of higher mean winds. A decreasing trend, dominated by a sharp decline beginning in 2005, is seen across China and the surrounding seas in summer and autumn, and the summer trends over land and over ocean appear to be related respectively to the Pacific Decadal Oscillation (PDO) and the East Asian summer monsoon. Trends are not consistent across the region in spring and winter, however, with positive trends over some areas in northeastern and northwestern China, Mongolia and tropical oceans whereas negative trends in other regions. Nearly all areas of China experience mean annual 80-m wind speed less than 6.9 m s^{-1} (wind power classes of 1–2) except for some areas of Inner Mongolia where mean annual 80-m wind speeds exceed 6.9 m s^{-1} (Classes 3 or higher, suitable for wind energy development). China Seas and ocean areas generally fall in Class 3 or above, with the Taiwan and Luzon Straights reaching the highest Class 7.

KEY WORDS wind energy; Pacific Decadal Oscillation; wind power resources in China; East Asian summer monsoon

Received 3 March 2015; Revised 15 June 2015; Accepted 20 July 2015

1. Introduction

Wind energy, as a renewable energy resource, has received much attention in recent years. Numerous investigations on wind energy potential and low-level wind distributions have been carried out for different regions around the world. Elliott *et al.* (1986, 2001a, 2001b, 2001c, 2002, 2003) produced a wind energy resource atlas for several countries around the world. Czisch and Ernst (2001) documented the potential annual wind energy production in Europe and its surrounding regions using the European Centre for Medium Range Weather Forecasts (ECMWF) Reanalysis-15 (ERA-15) data set. Archer and Jacobson (2003) assessed 80-m wind speeds in the continental United States based on wind observations at 1327 surface stations and 87 upper-air sounding sites for the year 2000. Yu *et al.* (2014) investigated the temporal and spatial variability of wind resources in the contiguous United States as derived from the Climate Forecast System Reanalysis (CFSR). McVicar *et al.* (2008) developed an Australia-wide daily near-surface wind speed data set at a resolution of 0.01° for the period of 1975 through 2006 using an expanded anemometer network. Most recently, Madhu and Payal (2014) reviewed studies on wind energy resources in India.

Besides wind energy over land areas, various studies have also examined wind resources offshore or over global oceans. For example, Pimenta *et al.* (2008) and Capps and Zender (2010) utilized the Quick Scatterometer (QuikSCAT) satellite data to evaluate the offshore wind power resource in southeastern Brazil for the August 1999 through June 2007 period and for the global ocean from January 2000 through December 2006. Zheng and Pan (2014) estimated global ocean wind power potential based on the Cross-Calibrated, Multi-Platform (CCMP) satellite wind fields for the period 1988–2011. In addition to satellite data, wind fields from global reanalyses have also been utilized to estimate wind power for the entire globe, including land and ocean areas (Archer and Jacobson, 2005; Lu *et al.*, 2009).

As the most populous country on earth and with its rapid economic development, China's demand on energy

* Correspondence to: S. Zhong, Department of Geography, Michigan State University, 673 Auditorium Rd., East Lansing, MI 48824, USA. E-mail: zhongs@msu.edu

has increased dramatically in the past two decades. There have been a number of studies on wind energy potential in China. A wind resource atlas for Southeast China was generated by Elliott *et al.* (2002). Based on hourly surface wind observations at four islands in the Pearl River Delta region, Zhou *et al.* (2006) noted considerable spatial and temporal variability of wind power potential over the region. By analysing wind observations from 395 surface stations around China, Liao *et al.* (2008) found that 2.51, 16.45, 53.39 and 27.65% of the total area in China falls in the class of wind energy density >150, 100–150, 50–100, and <50 W m^{-2}, respectively. McElroy *et al.* (2009) quantified the wind energy potential in China using wind data from the Goddard Earth Observing System Data Assimilation System Version 5 (GEOS-5 DAS) data set. Using the third-generation wave model, WAVEWATCH-III (WW3), Zheng *et al.* (2013) investigated offshore wind energy resources in the China Sea and found the richest area for wind energy is in the northern South China Sea, followed by the southern South China Sea and the East China Sea.

Apart from wind climatology, several studies have also examined trends in surface wind speed in China. Zuo *et al.* (2005) noted a decreasing trend in surface wind speed from 1961 to 2000 across most of the 62 meteorological stations in China. Wang *et al.* (2004) analysed 6-hourly surface wind speed data from 729 observational stations in China for the period of 1951 through 2000, and their results showed a decreasing trend over the entire country, which they attributed to the weakening East Asian monsoon. The association of decreasing surface wind speeds in China and the weakening of the East Asian monsoon has also been suggested by Xu *et al.* (2006) in their analyses of surface winds from 1969 to 2000; their study attributed the decline of the East Asian winter and summer monsoons to a combination of global-scale warming related to increased greenhouse gas emissions and local cooling resulting from air pollution. Niu *et al.* (2010) related the weakening of the East Asian winter monsoon to the regional increase in atmospheric aerosols. Besides the weakening of the East Asian monsoon, other reasons have also been suggested for decreasing surface wind speeds in China. Based on analyses of observations from 535 surface stations in China from 1956 to 2004, Jiang *et al.* (2010a) noted that urbanization and the change of anemometers or stations may have been mildly responsible for the decreasing trend in the annual mean wind speed, days of strong winds and maximum wind speeds. Guo *et al.* (2011) suggested that the primary cause for weakening surface winds is the decrease in the lower-tropospheric pressure-gradient, with urbanization playing a secondary role. Li *et al.* (2008) attributed decreasing surface wind speeds and near-surface wind power to urbanization and land-use change. Fu *et al.* (2011) and Lin *et al.* (2013) noted that the main decreasing trend occurs from 1979 to 2000 and attributed the decrease to latitudinal surface temperature gradient change and the interdecadal Pacific oscillation. Most recently, Jiang *et al.* (2013) linked decreasing maximum wind speeds in the coastal areas of Southeast China to the decreasing number and intensity of land-falling typhoons originating in the northwest Pacific Ocean.

In addition to the aforementioned studies on past wind speed trends in China and the surrounding oceans, studies have also examined the projected wind speed changes in China in the 21st century. Based on results from three regional climate models (RCMs), Jiang *et al.* (2010b) found that the projected annual and winter mean wind speeds in China will likely be lower during the 2081–2100 period than what was observed during the 1971–1990 period, while the projected changes in other seasons are less certain. In another study, Jiang *et al.* (2010c) examined the results of 19 global climate model (GCM) simulations from the Intergovernmental Panel on Climate Change (IPCC) Fourth Assessment Report (AR4) and found that the seasonal winds in the 21st century are likely to be weaker in winter and stronger in summer compared to those in the current climate represented by the period from 1980 to 1999. However, no significant changes in surface wind speeds were noted by Chen *et al.* (2012) in a study that compared winds from nine Coupled Model Intercomparison Project Phase 5 (CMIP-5) GCMs between the 2066–2100 and 1971–2005 periods. Jiang *et al.* (2013) suggested, based on projections from three GCMs of the IPCC AR4, that the annual and seasonal maximum wind speed will likely decrease for the 2046–2065 and 2080–2099 periods relative to the 1981–2000 period.

The aforementioned studies helped advance our understanding of the climatology of surface winds and wind energy resources in China and the China Seas. Few studies have focused on the spatial and temporal variability of seasonal wind energy resources over the region. Most studies of the trends in surface (10-m) wind speeds in China have relied on observational data from a network of surface weather stations (Wang *et al.*, 2004; Zuo *et al.*, 2005; Xu *et al.*, 2006; Niu *et al.*, 2010; Lin *et al.*, 2013). However, there is a concern in using surface station data for spatial analyses of wind variability in China because of the heterogeneity in the distribution of surface stations across China, with a high density of stations in the eastern portion of the country and a sparse distribution in the western and northwestern areas. Other studies using gridded data have employed global reanalyses that vary in horizontal resolution between 1° and 2.5° (approximately 100–250 km). While such resolutions may be sufficient for studies of wind resources over ocean surfaces and flat terrain, it may be inadequate to resolve spatial variations of wind over areas of complex terrain and heterogeneous land cover and land use.

In this study, we use a next-generation global reanalysis data set to revisit the wind climatology and wind resource distribution in China and the China Seas for the past three decades. The higher spatial resolution of the data set allows for a more accurate representation of low-level winds over the mountainous regions of southwestern China, the coastal regions of eastern China and the northwestern portion of the country where the observational stations are sparse. In addition to developing improved low-level wind climatology and wind resource maps with better spatial

resolution, the study also examines the trends in seasonal wind speeds and attempts to explain these trends.

The rest of the article is organized as follows. The data set and methods are described in Section 2. Section 3 presents the climatology, interannual standard deviation and trends in wind speeds in China, followed by an evaluation of wind power potential in China in Section 4. The results are summarized in Section 5 along with a discussion of the differences between our results and those from previous studies.

2. Data set and methods

This study investigates 80-m wind speeds over the region between 0°–55°N and 70°–140°E, covering all of China, the China Seas, the northern Indian Ocean, Mongolia and parts of southern and southeastern Asia (Figure 1). The data set used for this study is the CFSR (Saha *et al.*, 2010) produced by the US National Centers for Environmental Prediction (NCEP). Regarded as the next-generation global reanalysis, CFSR is a product of a global, high resolution, coupled atmosphere-ocean-land surface-sea ice system, which utilizes a suite of observational and model data (Saha *et al.*, 2010). In contrast to previous reanalysis products, new features of the CFSR include: the 6-h guess fields from a coupled atmosphere–ocean system, an interactive sea ice model, assimilation of satellite radiances over the entire period, and consideration of variations of carbon dioxide (CO_2), aerosols and other trace gases and solar activity. CFSR has an atmospheric resolution of ~38 km (T382) with 64 levels from the surface to 0.26 hPa, and an oceanic resolution of 0.25° at the equator and 0.5° beyond the tropics with 40 levels from the sea surface down to 4737 m. These resolutions are much higher both horizontally and vertically compared to the resolutions of earlier global reanalysis data sets. The global land surface model and the sea ice model of the CFSR have four and three levels, respectively. For details about the CFSR, refer to Saha *et al.* (2010).

Several studies have compared CFSR wind data to observations and to similar products in previous reanalysis data sets (Bao and Zhang, 2013; Rahim *et al.*, 2013; Chen *et al.*, 2014). In a recent study, Bao and Zhang (2013) compared winds from several global reanalysis data sets with those from rawinsonde soundings launched during the Tibetan Plateau Experiment (TIPEX) and found that winds from CFSR and the ERA-Interim agree better with the observations than those from the NCEP–National Center for Atmospheric Research (NCAR) global reanalysis and ERA-40. Rahim *et al.* (2013) found that the wind-speed correlation between CFSR and QuikSCAT over the South China Sea is 0.94 for the period from September 2008 through January 2009. Chen *et al.* (2014) assessed the diurnal cycle of wind fields from CFSR, ERA-Interim the Modern-Era Retrospective Analysis for Research and Applications (MERRA) and the 55-year Japanese Reanalysis (JRA-55) over eastern Asia by comparing them with the 6-hourly rawinsonde observations from 22 sites over

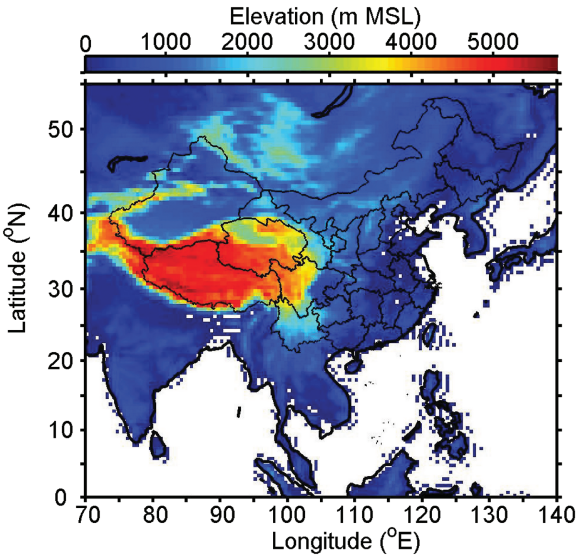

Figure 1. The study domain (0°–55°N, 70°–140°E) and the topography as resolved by the CFSR.

southern China. They noted that the four reanalysis data sets can represent the mean wind diurnal cycle, but they differ in the amplitude of the diurnal cycle.

This study utilizes the latest version of CFSR (CFSv2) (Saha *et al.*, 2014). The CFSv2 data archive has a temporal resolution of four times daily for the period of 1979 through 2011, and a vertical resolution of 25 hPa below 750 hPa and 50 hPa above 750 hPa, with 37 levels from 1000 to 100 hPa. At each grid point, the archived geopotential height fields are first subtracted from the terrain fields to obtain height above ground level (AGL). The 80-m level wind speed is then determined via a vertical linear interpolation between the CFSR archived 10-m winds and the winds at the geopotential height level just above 80 m. The interpolation is carried out for the meridional and zonal wind components, which are then used to compute wind speed. The same approach for obtaining 80-m wind speed was used by Li *et al.* (2010) in their analyses of wind resources in the Great Lakes region of the United States using the North American Regional Reanalysis (NARR). Li *et al.* (2010) compared the NARR 80-m wind obtained using linear interpolation with rawinsonde wind observations at five upper-air station locations over periods of 14–30 years and found good agreements with a bias within $\pm 0.6\ m\ s^{-1}$ among the five stations and an averaged bias across all five stations near zero. The 80-m level wind is derived for each of the four available times per day and the 6-hourly data are averaged to yield a daily mean, which is averaged further to obtain monthly and seasonal mean wind speeds.

In addition to CFSR data, the analyses also employed several indices for climate anomalies, including the Southern Oscillation Index (SOI) and Niño3.4 (http://www.cpc.ncep.noaa.gov/data/indices/), the multivariate El Niño Southern Oscillation (ENSO) Index (MEI) (http://www.esrl.noaa.goc/psd/enso/mei/), the East Asian Summer Monsoon Index (EASMI) (http://ljp.lasg.ac.cn/dct/page/

65577) (Li and Zeng, 2002, 2003), the Pacific Decadal Oscillation (PDO) index (Mantua *et al.*, 1997) and the Arctic Oscillation (AO) index (http://www.cpc.ncep.noaa.gov/data/indices).

3. Results

3.1. Domain-averaged wind

The 33-year mean annual cycle of daily mean 80-m winds averaged over the entire study region and several subregions are shown in Figure 2(a)–(e). Also shown in Figure 2(f)–(j) are the standard deviations of the mean for the corresponding regions. In all regions, the daily mean wind speeds follow a distinct seasonal cycle, but the patterns of variations vary between regions. When averaged over the tropical regions (Figure 2(b)) or the regions offshore (Figure 2(e)) within the study domain, the annual cycle exhibits a double peak (winter and summer) and double dip (spring and autumn) structure. Over the tropical regions, the two peaks are similar in magnitudes, and the dip in spring is slightly deeper than in autumn (Figure 2(b)). Similar to the tropical regions, the offshore regions also have minimum winds in spring, but the two maxima differ in magnitudes with higher values in winter than summer (Figure 2(e)). This double peak-dip structure is a reflection of the strong influence of the Southeast Asia Monsoon on the climate of these regions. In East Asia, the strength of the winter monsoon is typically stronger than that of the summer monsoon, and as a result, the strongest wind speeds usually occur in December and January. Winds are generally weaker in spring and autumn when the land–ocean thermal contrast is weak and the transition between winter and summer monsoons occur. The annual cycle exhibits a different seasonal variation pattern when averaged over extratropical regions (Figure 2(c)) or regions onshore (Figure 2(d)). In these regions, cold season (October–March) wind speeds are higher than warm season (April–September) winds, but the maximum and minimum over the two regions occur at different time of the year. Over the extratropical region, maximum winds are found in late winter and early spring and the minimum winds occur in mid to late summer (Figure 2(c)), but in the onshore region, peak wind speeds occur in mid-winter while the weakest winds occur in late summer and early autumn (Figure 2(d)). The averaged annual cycle for the entire domain (Figure 2(a)), which combines the features from the subregions, shows peak winds in winter and weak winds in autumn, with a secondary peak in early summer.

There are considerable variations of the standard deviations over the annual cycle, but in general, the standard deviations are larger in the tropical (Figure 2(g)) and offshore regions (Figure 2(j)) compared to the extratropical (Figure 2(h)) and onshore (Figure 2(i)) regions. Larger standard deviations suggest stronger interannual variability, which implies wind energy output in these regions would be more unpredictable. The interannual variability is further examined in Figure 3, which shows the time series of seasonal mean domain-averaged wind speeds for summer and winter. The time series for summer can be divided into two periods. During the first period, from 1979 to 2004, seasonal mean wind speeds over the study region oscillated around the 30-year mean of $4.89\,\mathrm{ms}^{-1}$. During the second period, from 2005 through 2011, seasonal mean wind speeds exhibited a decreasing trend of $-0.0624\,\mathrm{m\,s^{-1}\,year^{-1}}$. There is a strong correlation between the summer seasonal mean wind speed over the study region and the EASMI, with a correlation coefficient of 0.80. The summer time series is also correlated with Niño3.4, SOI and MEI, with correlation coefficients of 0.56, −0.61 and 0.51, respectively. During El Niño (La Niña) years, a positive (negative) wind speed anomaly occurs in the summer across the study region. The winter season mean wind speed varies between a maximum of $5.46\,\mathrm{m\,s^{-1}}$ in 1995 and a minimum of $4.97\,\mathrm{m\,s^{-1}}$ in 2010, with a mean of $5.24\,\mathrm{m\,s^{-1}}$. The wintertime mean wind speed over the study region seems to be related to the East Asian Winter Monsoon Index (Chen *et al.*, 2001), with a correlation coefficient of 0.53. Although no significant correlation is found between the winter season mean winds averaged across the entire domain and the AO index, the dominant mode of winter climate in mid- to high-latitudes in the Northern Hemisphere, winter season mean winds averaged over the extratropical region are correlated with the AO with a correlation coefficient of −0.38 at the 95% confidence level. The significant correlations of the seasonal mean winds to these global climate anomaly indicators could be used to improve wind energy forecasts at seasonal timescales or beyond.

The climatology, variability and trend of seasonal mean wind speed over land and ocean areas of the study region are shown in Figure 4 and Table 1. As expected, the seasonal mean wind speeds are stronger over ocean areas than over land throughout the year due to smaller friction over ocean areas. There is little seasonal variation over land, with wind speeds slightly stronger in spring and winter and weaker in summer and autumn. Winds over the ocean, however, exhibit a strong seasonal cycle with the strongest winds occurring in winter and the weakest winds occurring in spring. Winds over the ocean also show larger interannual variability for all seasons. Despite lower mean wind speeds over land relative to ocean, smaller seasonal and interannual variability and irregularity of wind speeds over land provide some good preconditions for stable wind energy production.

The trends of seasonal mean winds also differ somewhat between land and ocean (Table 1). Over land, there has been a significant (above 95% confidence level) downward trend ($-0.0087\,\mathrm{m\,s^{-1}\,year^{-1}}$) in summer. Over ocean areas, significant downward trends are seen in both summer ($-0.0088\,\mathrm{m\,s^{-1}\,year^{-1}}$) and autumn ($-0.0064\,\mathrm{m\,s^{-1}\,year^{-1}}$). No significant trends are detected for the other seasons. Similar to the domain-averaged summer mean winds (Figure 3(a)), the summer season mean winds over the ocean also exhibit two distinct periods (Figure 5(a)), with a positive trend of $0.0010\,\mathrm{m\,s^{-1}\,year^{-1}}$ (not significant) prior to the year 2005, and negative trend of $-0.0264\,\mathrm{m\,s^{-1}\,year^{-1}}$ (significant at above the

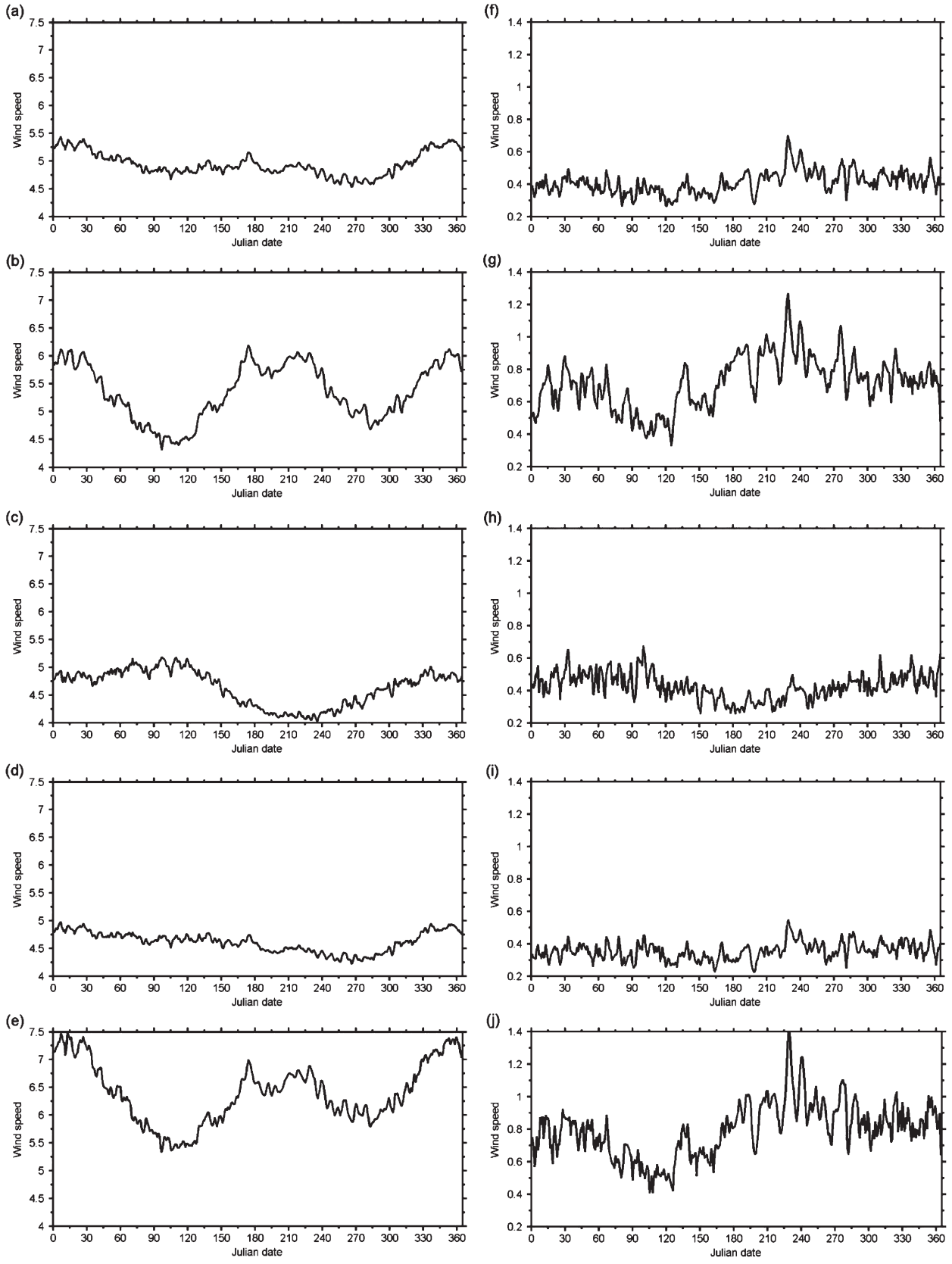

Figure 2. Time series of domain-averaged mean daily wind speed (a), (b), (c), (d) and (e) and standard deviation (f), (g), (h), (i) and (j) (unit: m s^{-1}). (a) and (f) for the whole region; (b) and (g) for the tropical region; (c) and (h) for the extratropical region; (d) and (i) for the offshore region; (e) and (j) for the onshore region.

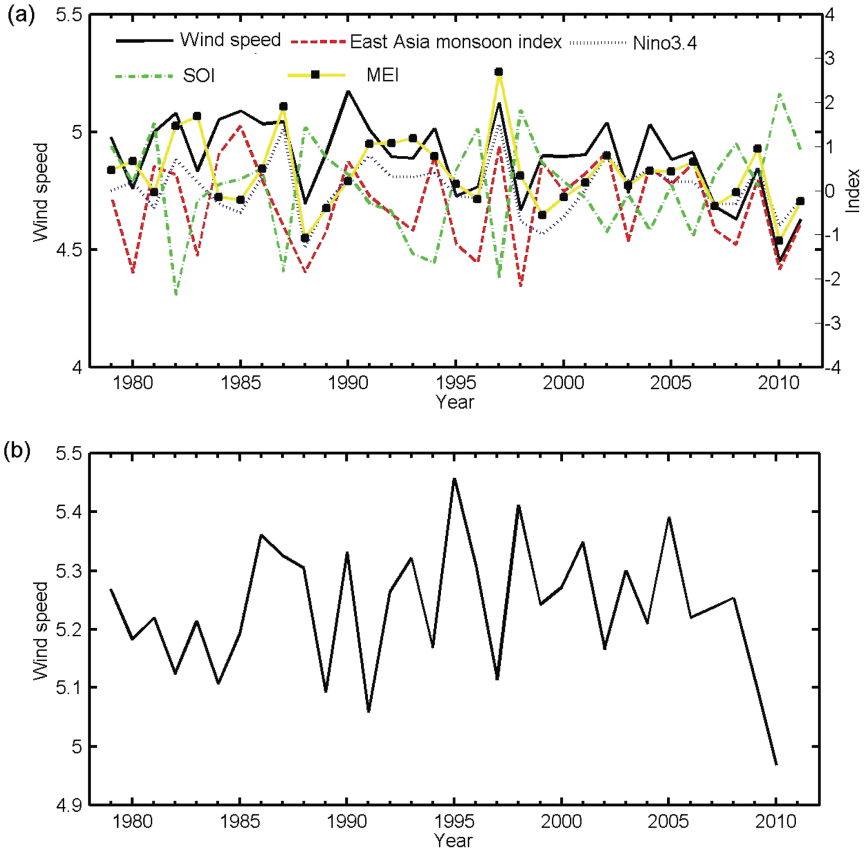

Figure 3. Domain-averaged seasonal mean 80-m wind speed (unit: m s^{-1}) (black), the East Asia monsoon index (red), the Niño 3.4 index (blue), the SOI index (green) and the MEI index (yellow) for summer (a) and winter (b).

95% confidence level) afterwards. The time series of the EASMI exhibits similar variability with a trend of 0.0027 $year^{-1}$ before 2004 and −0.0594 $year^{-1}$ after that (Figure 5(b)), suggesting a positive connection between the East Asian summer monsoons and the summertime mean wind speed over oceans in the study region. Over land, the mean wind in summer also exhibits two distinct periods before and after 1997 (Figure 6(a)). The average wind speed is 3.9 m s^{-1} before 1997 and 3.7 m s^{-1} afterwards. According to the MK abrupt change test (Mann, 1945), the time series has an abrupt change between 1997 and 1998 (Figure 6(b)). The abrupt summer season wind speed change before and after 1997 may be related to the abrupt change in the time series of the summertime PDO index that has the mean value of 0.87 before 1997 and −0.28 after 1997 (Figure 6(c)). The abrupt change of the PDO index also influences land and ocean temperatures, atmospheric carbon dioxide and ecosystems in the Pacific Ocean (Chavez *et al.*, 2003).

3.2. Spatial pattern

The domain-averaged wind speeds provide useful information on the temporal variability of wind across the study region as a whole. There is, however, large spatial variability across the domain given the complex topography, land cover and land use. Figures 7 and 8 depict the spatial distribution of seasonal mean wind speed averaged over the 33-year study period. In spring, strong westerly and northwesterly winds are seen over the Tibetan Plateau and Inner Mongolia of China and over eastern Mongolia, whereas weak winds occur over central and southern China and over southern and southeastern Asia (Figures 7(a) and 8(a)). Over the northern Indian Ocean, the cyclonic wind field surrounding India leads to high winds over the western Bay of Bengal. Easterly winds dominate the western Pacific Ocean and South China Sea. Northeasterly winds from an anticyclonic cell over the Yellow Sea and easterly winds from the western Pacific Ocean converge over the Taiwan Strait, leading to high winds exceeding 9 m s^{-1}. Winds exceeding 9 m s^{-1} also occur over regions south of Japan.

In summer, wind speeds over Inner Mongolia of China and eastern Mongolia remain high. High wind speeds also occur over western China, in particular, over the Xinjiang Autonomous region as well as over southern India and Sri Lanka (Figure 7(b)). The strong winds over Xinjiang may be due largely to terrain, reflecting westerly flow deflected by the Tian Mountain, whereas high winds over southern India and Sri Lanka can be attributed largely to the onset of the South Asian monsoon (Figure 8(b)). The prevailing South Asian monsoon also generates westerly and southwesterly winds, leading to wind speeds exceeding 10 m s^{-1} with a maximum value of 12.9 m s^{-1} over the northern Indian Ocean. Regions of the China Seas and the western Pacific Ocean are characterized mainly by

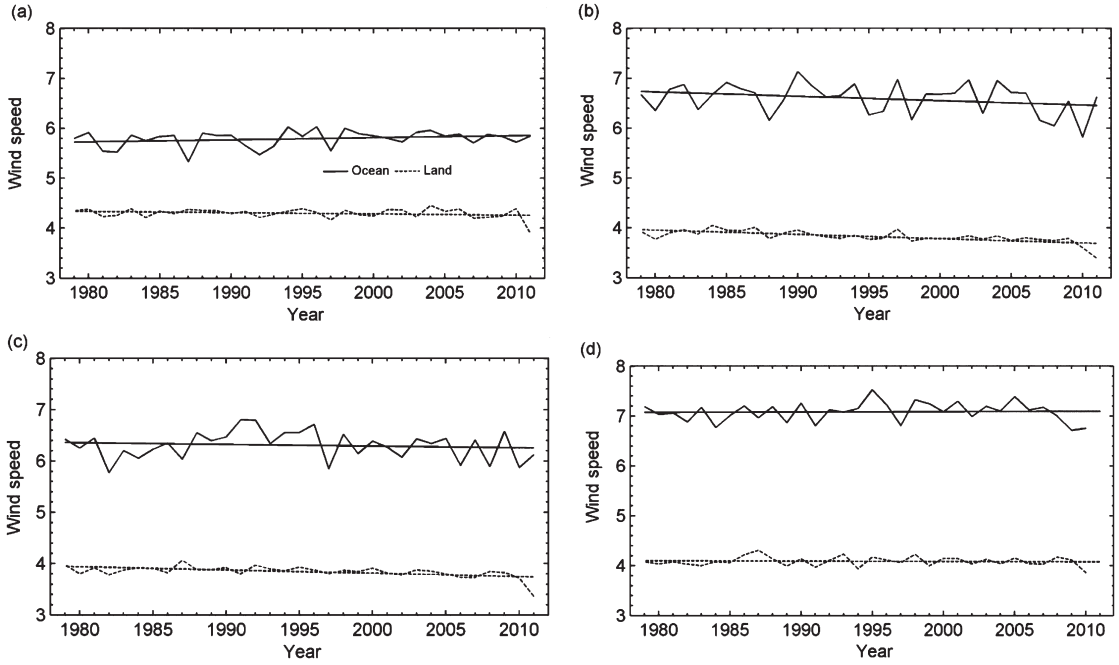

Figure 4. Seasonal mean wind speed averaged over land (solid line) and ocean (dotted line) for the 33-year period of 1979–2011 for spring (a), summer (b), fall (c) and winter (d). The straight solid line indicates the linear trend.

Table 1. The climatology ($m\,s^{-1}$), interannual standard deviation (STD) ($m\,s^{-1}$) and trend of seasonal wind speed ($m\,s^{-1}\,year^{-1}$) over land and ocean in the study region for the period of 1979 through 2011. The asterisk indicates the significance of the trend is above the 95% confidence level.

	Spring	Summer	Fall	Winter
Climatology (land)	4.30	3.83	3.84	4.09
Climatology (ocean)	5.79	6.59	6.31	7.09
STD (land)	0.10	0.12	0.11	0.09
STD (ocean)	0.16	0.31	0.27	0.19
Trend (land)	−0.0026	−0.0087*	−0.0033	0.0007
Trend (ocean)	0.0042	−0.0088*	−0.0064*	−0.0007

southerly winds. It is interesting to note that the strong East Asian summer monsoons do not produce strong winds over most of eastern China and southeastern Asia.

In autumn, the end of the South Asian summer monsoon weakens winds over India and over the northern Indian Ocean (Figures 7(c) and 8(c)). But the onset of the East Asian winter monsoon helps strengthen winds over northeastern China, with maximum speeds occurring over Inner Mongolia. Easterly and northeasterly winds dominate the China Seas and the western Pacific Ocean. Relatively strong winds occur over the Taiwan Strait, the Luzon Strait and the northeastern South China Sea, with a maximum wind speed of $12.5\,m\,s^{-1}$.

The winter season wind pattern shows the influence of the winter monsoon and the strengthening of westerly winds over the Tibetan Plateau (Figures 7(d) and 8(d)). Winds in eastern Mongolia and Inner Mongolia of China remain high. The wind fields over the China Seas and the western Pacific Ocean are similar to the spatial pattern in autumn, but the wind speeds are generally stronger. Relatively high winds are found over the South China Sea, Taiwan and Luzon Straits, Japan Sea and the region south of Japan. A maximum winter season mean wind speed of $13.7\,m\,s^{-1}$ is found over the Taiwan Strait.

The spatial distributions of the interannual variability for the four seasons are shown in Figure 9. Over land, larger interannual variations in seasonal mean wind speed are found over the Tibetan Plateau, Mongolia and Inner Mongolia of China for all seasons, though the values exhibit seasonal dependency. For example, the interannual variability over the Tibetan Plateau is at a maximum in winter and at a minimum in autumn. The large interannual variability of winter winds over the Tibetan Plateau is likely to be related to the variability in the location and strength of the westerly jet over this region (Schiemann *et al.*, 2009). Winds in Mongolia show stronger interannual standard deviation in summer and autumn. Kurosaki *et al.* (2009) attributed the interannual variability of wind speed to land-cover and land-use changes (e.g. vegetation cover, snow cover, frozen soil, cultivation and grazing). Winds in the region north of Lake Balkahash also exhibit relatively large interannual variability in winter.

Over the ocean, interannual variability is weakest in the spring with higher values over the western Pacific Ocean, the South China Sea and also over the northern Indian Ocean where a maximum value of $1.07\,m\,s^{-1}$ is found. In summer, strong interannual variations in the Asian summer monsoon (Li, 2010) result in large interannual variability of winds over the tropical oceans, with a maximum value of $1.54\,m\,s^{-1}$ found over the western tropical Pacific Ocean. In autumn, larger interannual variability occurs mainly over the northern Indian Ocean, with a maximum value of $1.19\,m\,s^{-1}$. Finally in winter, large

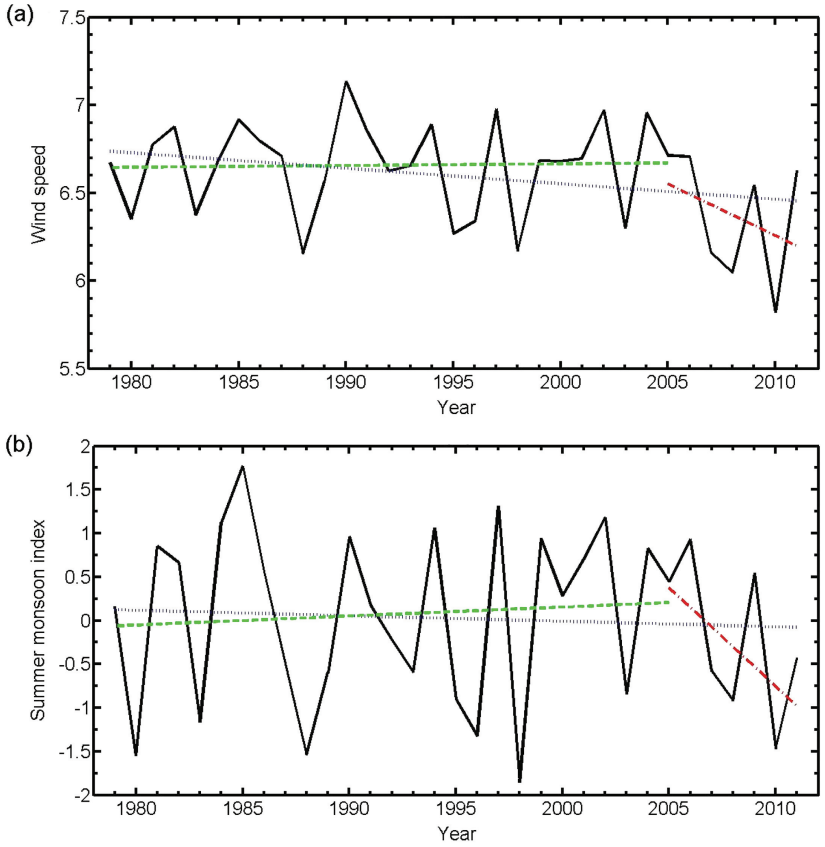

Figure 5. The time series of domain-averaged summertime mean wind speed averaged over the ocean (a) and the East Asian summer monsoon index (b) for the 33-year period of 1979–2011. The blue, green and red lines indicate the total trends, trends prior to 2005 and trends after 2005, respectively.

variability with a maximum value of 1.21 m s^{-1} occurs over the South China Sea and the western Pacific Ocean, which are regions affected by cold surges related to the East Asian winter monsoon (Zhang *et al.*, 1997).

To further understand how the seasonal mean wind speed has changed over the course of the 33 years, linear regression analysis was performed for the 33 seasonal mean wind speed values at each grid point in the study domain. Figure 10 shows the slope of regression (i.e. the trend) that exceeded the 95% confidence level for the entire domain. To help explain the trend, linear regression analysis was also performed for the sea-level pressure and the 80-m wind vector field. The slopes of these regressions are shown in Figures 11 and 12.

The spring season winds show negative trends over Mongolia, the Tibetan Plateau, southern China, India and the western Bay of Bengal (Figure 10(a)). The negative trends over Mongolia appear to be related to the easterly winds induced by the positive trend in the sea-level pressure over the region (Figures 11(a) and 12(a)), which oppose the climatological westerly winds (Figure 8(a)). A similar explanation can be applied to other regions where the trends are negative. Positive trends, on the other hand, occur over the Japan Sea, the South China Sea, the eastern Bay of Bengal and part of the western Pacific Ocean, where the direction of the wind vector field is the same as that of the climatological wind field. These positive trends, with a maximum value of 0.05 m s^{-1} year^{-1}, are more significant in spring than the rest of the year.

In summer, negative trends prevail with larger values over western and northeastern China, Mongolia, the Bo Sea, part of the Yellow Sea and the northern Indian Ocean (Figure 10(b)). The extent of the spring season positive trend in sea-level pressure over Mongolia (Figure 11(b)) induces the trend of easterly winds over Mongolia and northerly winds over eastern China, which are opposite to the climatological wind directions in these regions (Figure 12(b)) and lead to the negative wind speed trend over the region. The negative trend over the Tibetan Plateau can be explained by the trend of easterly winds that are opposite to the westerly climatological winds in this region. This also occurs over the northern Indian Ocean where the differences in the sea-level pressure trends between India and the Bay of Bengal and the northern Indian Ocean lead to a trend of easterly winds that oppose the westerly climatological winds in the region. Small areas of positive trends are scattered over northwestern China and the western Pacific Ocean.

In autumn, the trends remain generally negative across the domain, but areas with significant negative trends (e.g. western China and the northern Indian Ocean) are less extensive compared to the pattern in the summer (Figure 10(c)). Significant negative trends can be seen over Mongolia and south of Sri Lanka (Figure 10(c)), both of

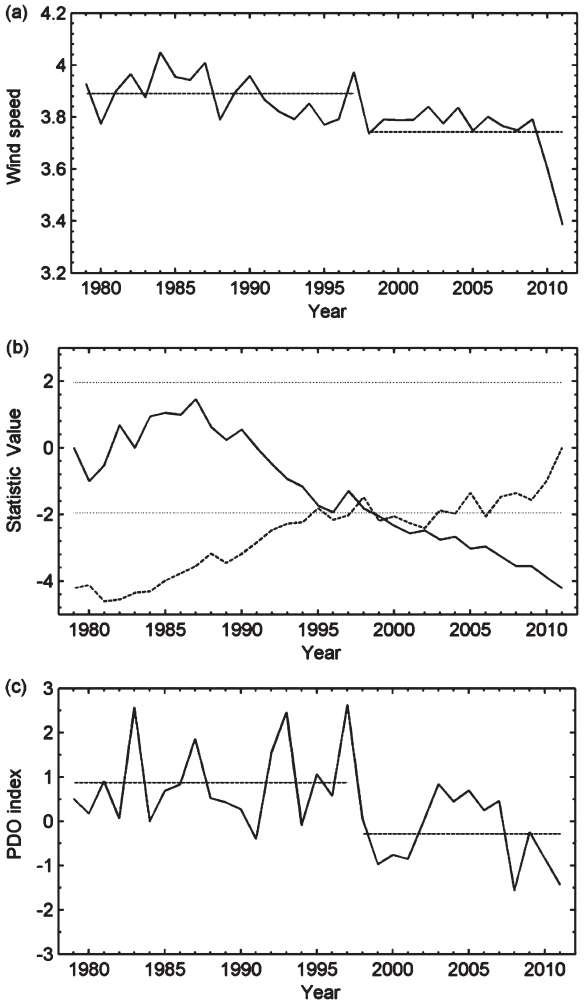

Figure 6. The time series of domain-averaged summertime mean wind speed averaged over land (a), MK abrupt change statistical test (b) and the time series of the summertime PDO index (c). The dashed lines in (a) and (c) indicate the mean values before and after 1997. The dotted horizontal lines in (b) correspond to ±1.96 indicating the 95% confidence level.

which can be explained by the significant easterly wind trends in the region (Figure 12(c)).

Finally, significant negative trends in winter are located over Mongolia, with smaller areal coverage compared to the coverage in autumn. Negative trends also characterize the southern parts of the South China Sea (Figure 10(d)), which are related to the southwesterly wind trend over the region (Figure 12(d)) and are nearly opposite to the climatological wind field there. Positive trends are found over northern Mongolia and in areas of northwestern and northeastern China. In addition, positive trends also occur over the sea near Sri Lanka and south of Japan. These positive trends can be explained by comparing the vector wind trends in Figure 12(d) with the climatological winds in Figure 8(d), where the wind directions are consistent in these regions.

Several previous studies have showed an overall decreasing trend in wind speed in China and attributed it to the weakening of the East Asian summer and winter monsoons. This study shows that the decreasing trend across China is most significant in summer, followed by autumn and least significant in winter. The decreasing trend in summer is likely related to changes in the PDO (Figure 6). In spring and winter, there is a significant increasing trend in the wind speed over northern China (Figure 10(a) and (d)). The increasing trend in wind speed over northern China and the Bo Sea is related to the trend of increasing northerly winds induced by the positive trend in sea-level pressure over Mongolia (Figure 12(d)). The difference in the sea-level pressure trends between northern and southern China also contributes to the positive trend in wind speed over northern China (Figure 11(d)). Chen *et al.* (2001) showed an increasing trend of 0.0079 year^{-1} in the East Asian winter monsoon index, though the trend is not significant at the 95% confidence level.

A word of caution is in order when the results of the trends of mean wind speed are applied to wind energy production because a decreasing or an increasing trend in mean wind speed does not necessarily imply a decreasing or an increasing trend in wind energy production. In addition to the mean annual wind speed, another important consideration is the distribution of the wind speed spectrum that influences wind energy production. For example, despite a decrease in mean wind speed, an increase in the upper wind speed percentile in the wind speed spectrum may lead to enhanced wind energy production. Vertical wind shear near the ground, directional variability and turbulence intensity also can impact the wind energy output. The spatial and temporal variability of air density related to air temperature and humidity can also exert an impact on wind energy production (Pryor and Barthelmie, 2011).

4. Wind power potential

A seven-class system, based on the mean annual 80-m wind speed, has been used widely to rank wind power resources (Archer and Jacobson, 2003, 2005; Li *et al.*, 2010) (Table 2). Class 1, defined as 80-m mean annual wind speeds of less than 5.9 m s^{-1}, is considered unsuitable for wind power development. Class 2, corresponding to mean wind speeds between 5.9 and 6.8 m s^{-1}, is regarded as marginal. Finally, Class 3 and above corresponding to mean wind speeds equal to or greater than 6.9 m s^{-1}, is considered suitable. Using the mean annual wind speed at each grid point in the study domain, we calculated the percentage of years during the 33-year study period when the grid point falls under each of the seven classes. Figure 13 shows the spatial distribution of the percentages separated by class. The majority of land points fall under Class 1. The land grid points that fall under Class 2 in some years are found in areas north of Lake Balkhash, southern Mongolia and Inner Mongolia of China, and over the Tibetan Plateau although only scattered areas over the Plateau have percentages >50%. A small number of land points, located mainly over southern Mongolia and central Inner Mongolia of China, fall under Classes ≥3 and this occurs at <30% of the time except for a few locations where the percentage exceeds 50%. Most of the ocean

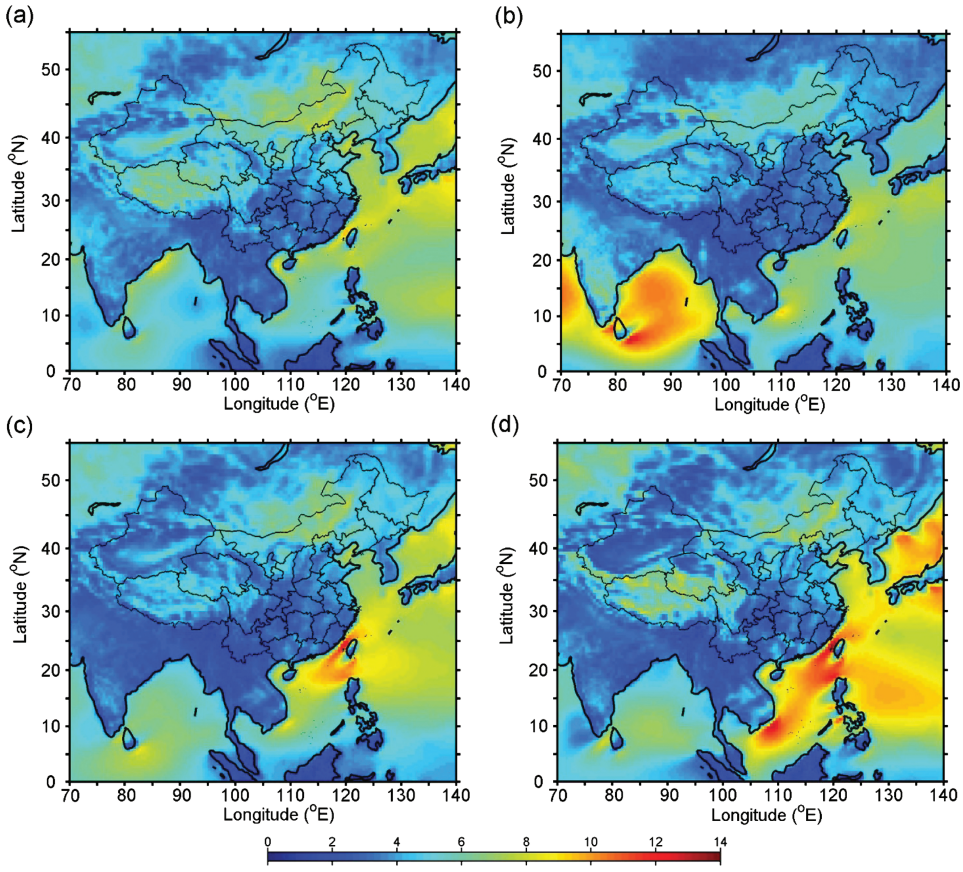

Figure 7. Seasonal mean wind speed (unit: m s^{-1}) averaged from 1979 to 2011 over the study domain for spring (a), summer (b), fall (c) and winter (d).

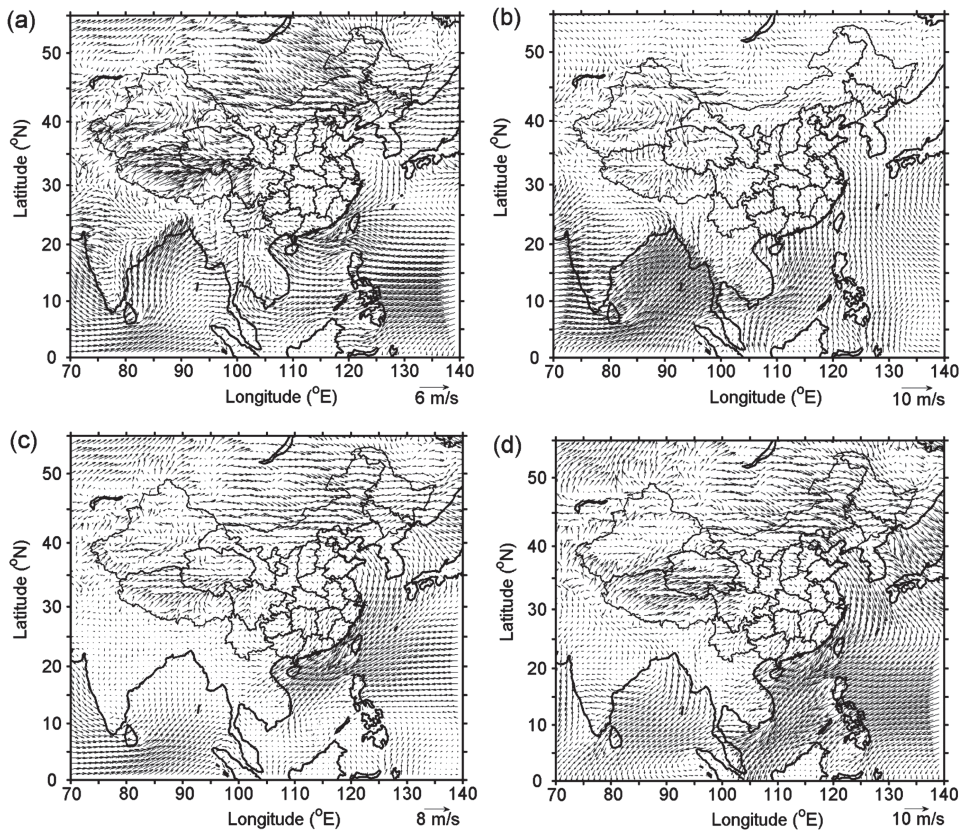

Figure 8. Seasonal mean wind field averaged from 1979 to 2011 over the study domain for spring (a), summer (b), fall (c) and winter (d).

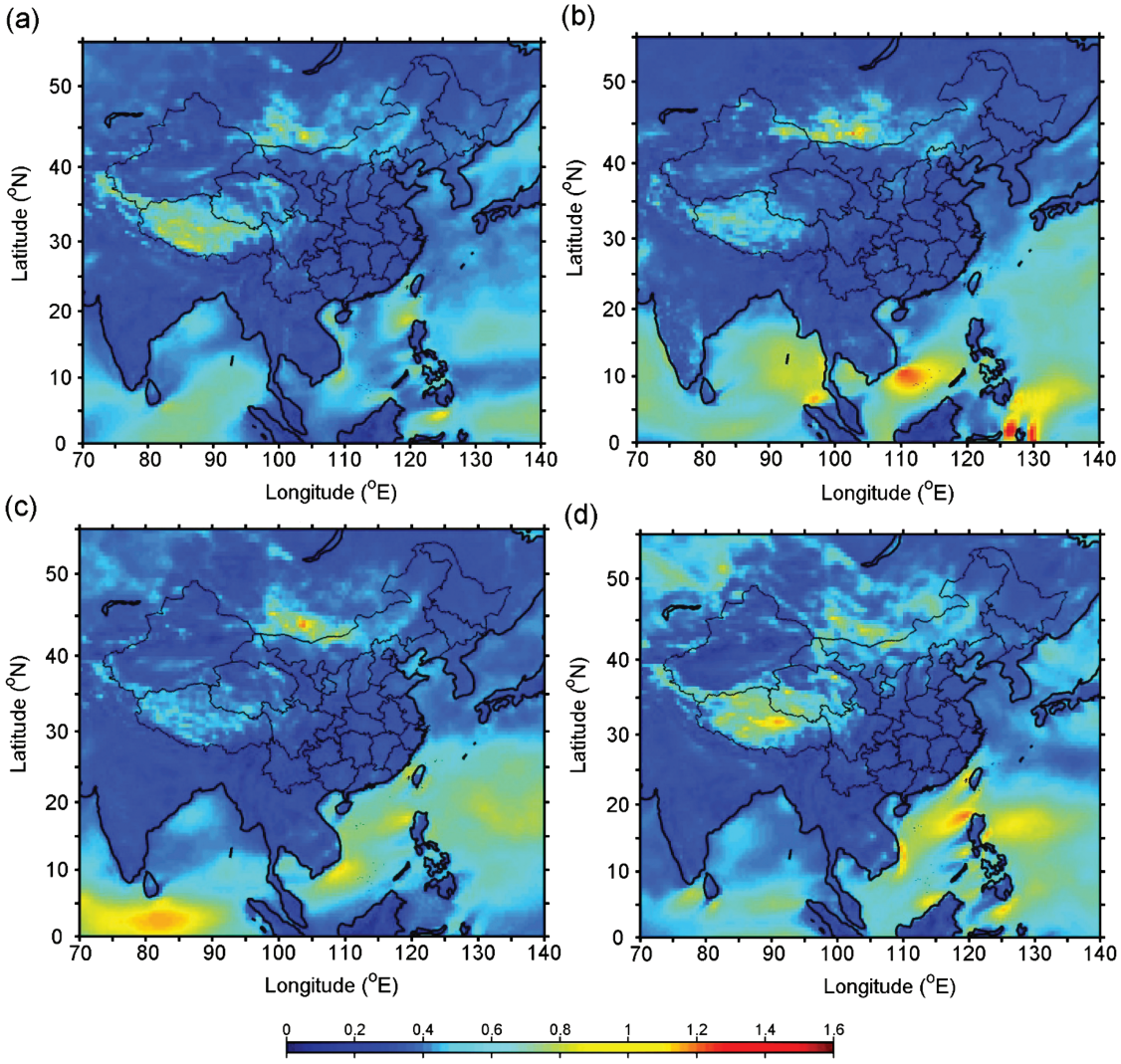

Figure 9. Interannual standard deviation of seasonal mean wind speed (unit: m s^{-1}) from 1979 to 2011 over the study domain for spring (a), summer (b), fall (c) and winter (d).

grid points, however, fall under Classes ≥2 at >80% of the time. Grid points over the Bo Sea and Yellow Sea fall into Classes 2 and 3, those over the East Sea fall into Classes 4 and 5 and those over the Japan Sea fall into Classes ≥3. Most of the South China Sea and the northwestern Pacific Ocean also fall into Classes ≥3.

Figure 14 shows the wind class for each grid point in the study domain based on the 33-year averaged annual mean 80-m wind speed computed from the CFSR. Among the total of 15 651 CFSR grid points in the region, 11 011 grid points (70.35%) fall into Class 1, 1698 grid points (10.85%) belong to Class 2 and 1517 grid points (9.69%) are in Class 3. Among the 1517 Class 3 grid points, only 21 are over land (Inner Mongolia of China). Finally, 1012 (6.47%), 304 (1.94%), 96 (0.61%) and 13 (0.08%) grid points fall into Classes 4, 5, 6 and 7, respectively. All 13 grid points in Class 7 are located over the Taiwan Strait.

These results confirmed the findings from earlier studies that of all regions in China, Inner Mongolia offers the richest wind sources for wind energy development, followed by Tibet (McElroy *et al.*, 2009). However, as shown earlier, winds over the Tibet Plateau experience considerable interannual variability especially in spring and winter, potentially affecting the stable output of wind energy. The negative trends in seasonal mean wind speed in summer and autumn over northern China and in spring and summer over Tibet provide additional information for the planning of wind energy development. This study also shows that the coastal areas of southeastern China are rich in wind resources , as was first suggested by Elliott *et al.* (2002). The southerly winds in summer and the northeasterly winds in other seasons speed up through the Taiwan Strait, boosting the wind energy class there to reach Class 7. Zheng and Pan (2014) also found rich wind resources over the Taiwan Strait, but underestimated the wind energy class. Their study identified the Luzon Strait as the richest resource for wind energy over the China Sea, which falls into Class 6 in our results. Despite these local differences in specific wind energy classes, the overall pattern of wind energy distribution over the China Sea identified in this study is similar to the pattern identified by Zheng and Pan (2014).

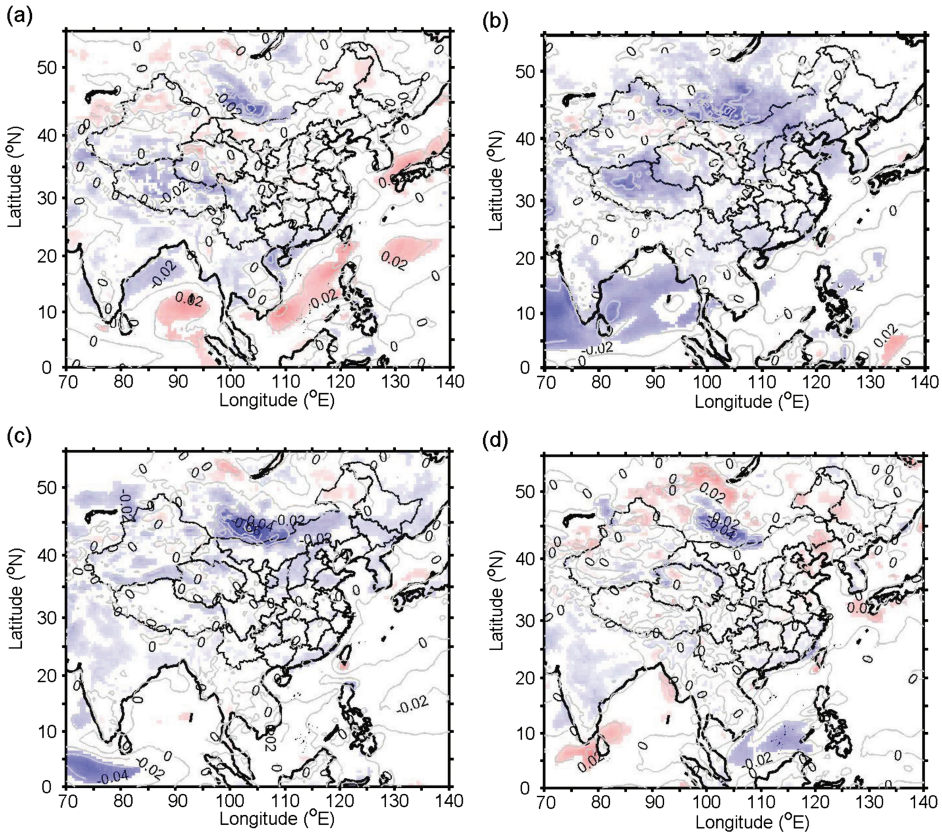

Figure 10. Trends in seasonal mean wind speed (unit: m s^{-1} $year^{-1}$) from 1979 to 2011 over the study domain for spring (a), summer (b), fall (c) and winter (d). The filled regions are significant at the 95% confidence level.

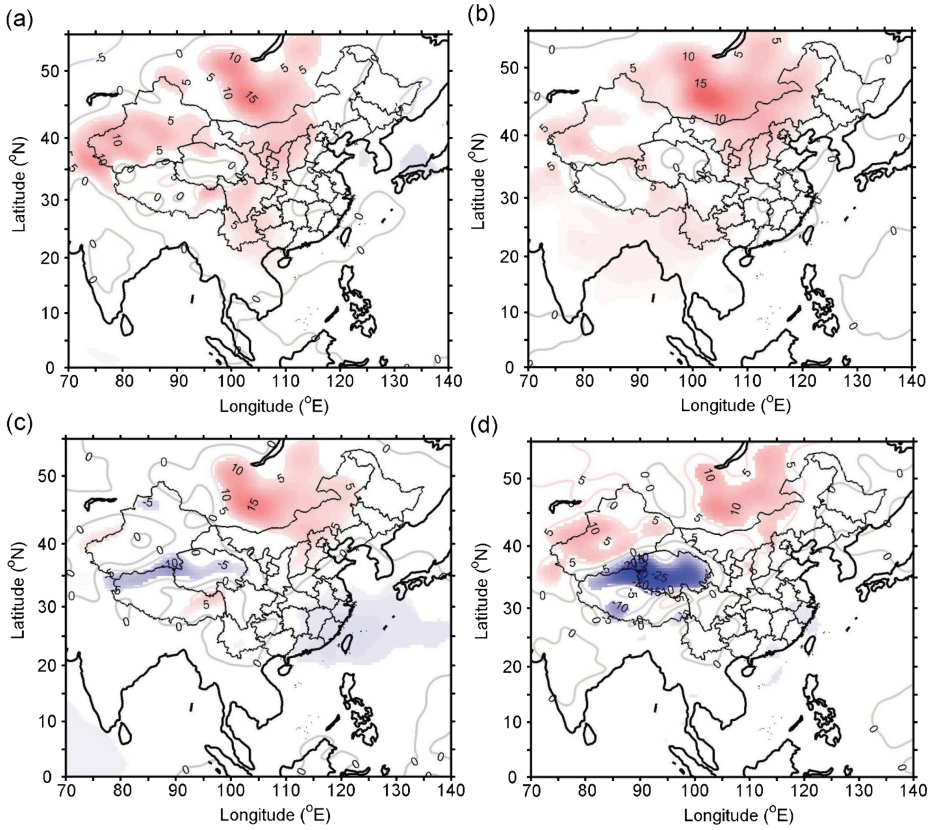

Figure 11. Trends in seasonal mean sea-level pressure (unit: Pa $year^{-1}$) from 1979 to 2011 over the study domain for spring (a), summer (b), fall (c) and winter (d). The filled regions are significant at the 95%

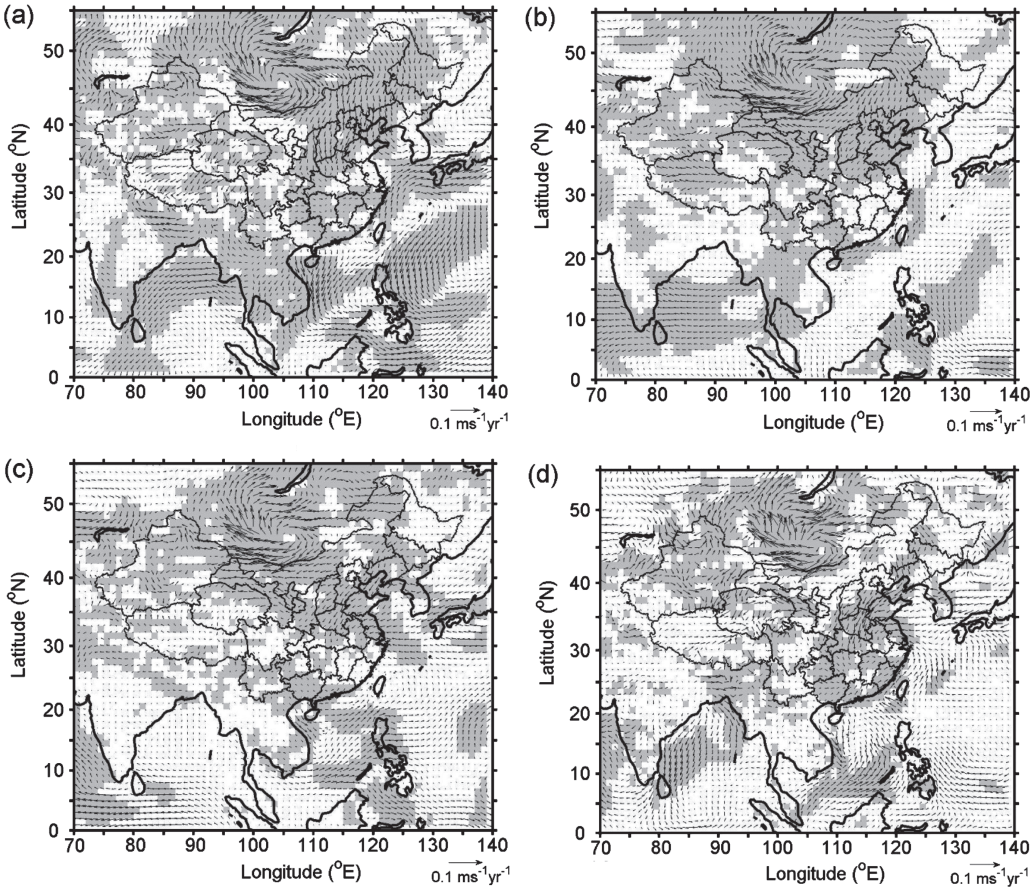

Figure 12. Trends in seasonal mean wind field from 1979 to 2011 over the study domain for spring (a), summer (b), fall (c) and winter (d). The shaded regions are significant at the 95% confidence level.

Table 2. Wind speeds corresponding to different wind power classes at 80 m (Archer and Jacobson, 2003).

Class	Wind speed at 80 m AGL ($m\,s^{-1}$)	Suitability for wind power
1	$V < 5.9$	Unsuitable
2	$5.9 \le V < 6.9$	Marginal
3	$6.9 \le V < 7.5$	Suitable
4	$7.5 \le V < 8.1$	Suitable
5	$8.1 \le V < 8.6$	Suitable
6	$8.6 \le V < 9.4$	Suitable
7	$V \ge 9.4$	Suitable

5. Summary and discussion

This study utilized the next-generation CFSR data over a 33-year period from 1979 through 2011 to develop a spatially improved climatology of winds at the hub height (80 m AGL) of modern wind turbines over China and the China Seas. The results confirmed some of the major findings from several previous studies that were based either on data from surface weather stations or from earlier global reanalysis data sets that have coarser spatial resolution. The results also shed light on the mechanisms for the trends and interannual variability in wind energy resources.

The results revealed substantial seasonal variations of 80-m winds for the study region as a whole. Stronger mean winds occur in winter and summer in association with the monsoon climate of eastern and southern Asia. Daily, seasonal and annual mean wind speeds vary substantially across the region. At all timescales, winds over water are consistently stronger than over land. Over land areas, higher winds occur in southern Mongolia, Inner Mongolia of China and areas over the Tibetan Plateau, whereas higher winds are seen over the northern Indian Ocean in summer in association with westerly winds, and over the East China Sea, South China Sea, Japan Sea and the western Pacific Ocean in connection to northwesterly and northeasterly winds.

Across the region, winds exhibit strong seasonal variability. Although the patterns of the seasonal variations vary from region to region, the strong influence of the Southeast Asia Monsoon cycle on the region's climate results in generally higher winds in winter, which is followed by summer, when the ocean–land thermal contrasts are large. Weaker winds occur in autumn and spring when the transitions between winter and summer monsoons occur. The seasonal and annual mean wind speeds show significant interannual variability. The amplitudes of the interannual variability are consistently larger over oceans than over land areas and in general the regions with stronger interannual variability coincide with the regions of higher mean winds. The summer season mean winds

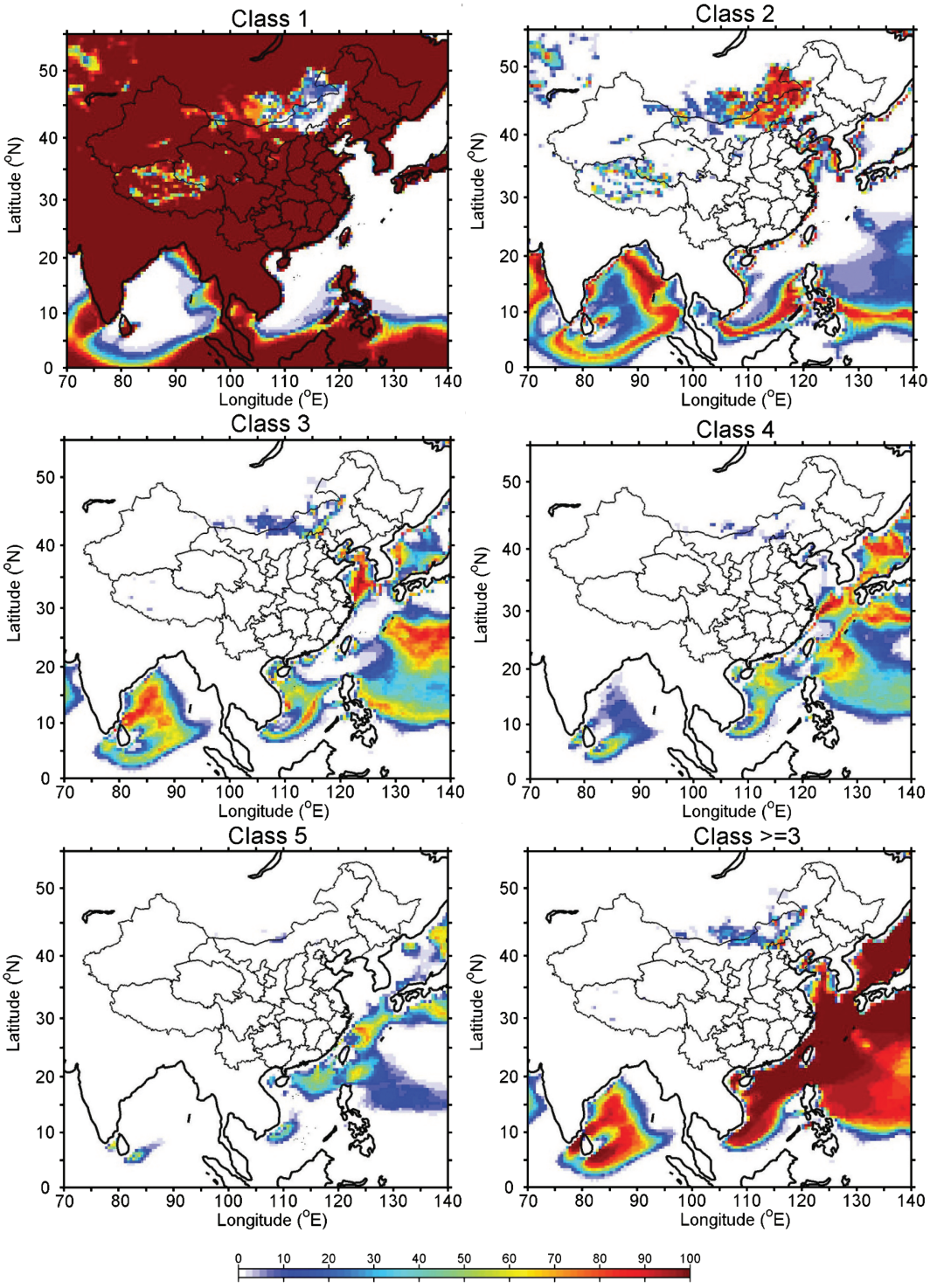

Figure 13. The percentage of years when the annual mean wind speeds fall into each wind power class.

over the study region shows a strong positive correlation with the EASMI (correlation coefficient, $r = 0.80$) and the Niño3.4 and MEI ($r = 0.56$ and 0.51) indices, and a negative correlation with the SOI index ($r = -0.61$). The winter season mean winds, when averaged over the entire region, are positively correlated with the East Asian winter monsoon index ($r = 0.53$), and when averaged over the extratropical areas, are negatively correlated with the AO index ($r = -0.38$).

The statistically significant negative trends in the domain-averaged 80-m wind speed in summer over land and over ocean appear to be associated with the changes in the summertime PDO and the East Asian summer monsoon, respectively. Negative trends in summer occur over most of China, Mongolia and the northern Indian Ocean. While negative trends are also seen over the same geographic locations in autumn, the areal extent is considerably reduced from the extent in summer.

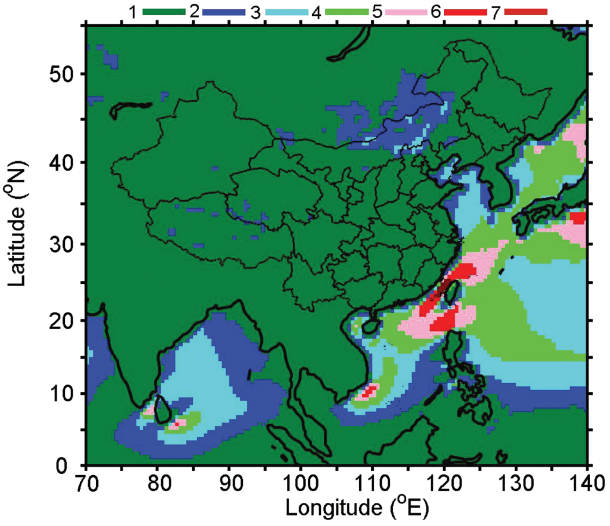

Figure 14. The climatology of wind power class for each grid point in the study domain as determined from the 33-year averaged annual mean 80-m level wind speed from CFSR.

Positive trends in wind speed occur mainly in spring and winter and are located over northwestern and northeastern China, northern Mongolia and the surrounding seas and oceans.

Nearly all areas in China experience mean annual wind speed at the 80-m height level that are less than 6.9 m s^{-1}, which corresponds to wind power classes of 1–2. The exception to this can be found in areas of Inner Mongolia where mean annual 80-m wind speeds are greater than 6.9 m s^{-1}, which corresponds to wind power classes of 3 or higher. In contrast, the majority of surrounding ocean areas have mean annual 80-m wind speeds that fall into Class 3 or above, with the Taiwan and Luzon Straights reaching the highest Class 7. A wind power class of 3 or above is generally considered to have wind resources suitable for utility-scale wind power development, although some suitable sites also exist in areas with Classes 1 and 2.

It is important to point out that the wind speeds used for this assessment, which represent averaged wind speeds over an area of 38 km^2, are likely to underestimate the actual winds in some areas within the grid box especially hilltops, ridge crests and mountain summits where winds are usually higher than the surroundings. The grid-averaged winds are also likely to be an underestimate of actual winds in coastal areas because of the underestimation of sea and land breezes. In other areas, surface heterogeneities can lead to an underestimation of thermally induced secondary circulations.

Finally, it is worth mentioning the study shortcomings. First, as just discussed above, although the CFSR data set is a substantial improvement over the first generation reanalysis data set such as the NCEP-NCAR global reanalysis and the NCEP-DOE global reanalysis II, they are still relatively coarse in resolution. Wind speeds at local scales smaller than the nominal resolution of 38 km of the CFSR grid cells are not represented well by the wind speeds at CFSR grid points. Second, as discussed earlier, the positive trend in wind speed in winter over northern China disagrees with previous results, and understanding the reasons for the discrepancy requires further analysis. Third, the relationship between summertime wind speed over land and the summertime PDO index also warrants further investigation. Finally, this study only analysed the interannual standard deviations of seasonal mean wind speed over China and its surrounding regions and briefly explored their relationship to large-scale circulation anomalies; a full understanding of the relationships between the interannual variability of the mean wind speed and dominant modes of global climate anomalies requires further study with more in-depth analyses.

Despite these limitations, the results about seasonal variations and trends in 80-m wind speed and their spatial distributions should prove useful for the wind energy industry and energy policymakers.

Acknowledgements

The authors thank NCEP for producing CFSR data. This research is supported by the National Science Foundation of China (41401017), the Open Foundation of State Key Laboratory of Hydrology-Water Resources and Hydraulic Engineering (2014490911), and by the AgBioResearch of Michigan State University.

References

Archer CL, Jacobson MZ. 2003. Spatial and temporal distributions of U.S. winds and wind power at 80 m derived from measurements. *J. Geophys. Res.* **108**: 4289, doi: 10.1029/2002JD002076.

Archer CL, Jacobson MZ. 2005. Evaluation of global wind power. *J. Geophys. Res.* **110**: D12110, doi: 10.1029/2004JD005462.

Bao X, Zhang F. 2013. Evaluation of NCEP-CFSR, NCEP-NCAR, ERA-Interim, and ERA-40 reanalysis datasets against independent sounding observations over the Tibetan Plateau. *J. Clim.* **26**: 206–214.

Capps SB, Zender CS. 2010. Estimated global ocean wind power potential from QuikSCAT observations, accounting for turbine characteristics and sitting. *J. Geophys. Res.* **115**: D09101, doi: 10.1029/2009JD012679.

Chavez FP, Ryan J, Lluch-Cota SE, Ñiquen CM. 2003. From anchovies to sardine sand back: multidecadal change in the Pacific Ocean. *Science* **299**: 217–221.

Chen W, Graf HF, Huang RH. 2001. The interannual variability of East Asian winter monsoon and its relation to the summer monsoon. *Adv. Atmos. Sci.* **17**: 48–60.

Chen L, Pryor SC, Li D. 2012. Assessing the performance of Intergovernmental Panel on Climate Change AR5 climate models in simulating and projecting wind speeds over China. *J. Geophys. Res.* **117**: D24102, doi: 10.1029/2012JD017533.

Chen G, Iwasaki T, Qin H, Sha W. 2014. Evaluation of the warm-season diurnal variability over East Asia in recent reanalyses JRA-55, ERA-Interim, NCEP CFSR, and NASA MERRA. *J. Clim.* **27**: 5517–5537.

Czisch G, Ernst B. 2001. *High Wind Power Penetration by the Systematic Use of Smoothing Effects within Huge Catchment Areas Shown in a European Example, Wind Power 2001*. American Wind Energy Association: Washington, DC.

Elliott D, Holladay CG, Barchet WR, Foote HP, Sandusky WF. 1986. Wind energy resource atlas of the United States. U.S. Department of Energy Report DOE/CH10093-4, U.S. Department of Energy, Washington, DC, 210 pp.

Elliott D, Schwartz M, George R, Haymes S, Heimiller D, Scott G, Kline J. 2001a. Wind energy resource atlas of the Dominician Republic. NREL/TP-500-27602, National Renewable Energy Laboratory, Golden, CO.

Elliott D, Schwartz M, Scott G, Haymes S, Heimiller D, George R. 2001b. Wind energy resource atlas of Mongolia. NREL/TP-500-28972, National Renewable Energy Laboratory, Golden, CO.

Elliott D, Schwartz M, George R, Haymes S, Heimiller D, Scott G, McCarthy E. 2001c. Wind energy resource atlas of the Philippines. NREL/TP-500-26129, National Renewable Energy Laboratory, Golden, CO.

Elliott D, Schwartz M, Scott G, Haymes S, Heimiller D, George R. 2002. Wind energy resource atlas of Southeast China. NREL/TP-500-32781, National Renewable Energy Laboratory, Golden, CO.

Elliott D, Schwartz M, Scott G, Haymes S, Heimiller D, George R. 2003. Wind energy resource atlas of Armenia. NREL/TP-500-33544, National Renewable Energy Laboratory, Golden, Colorado.

Fu G, Yu J, Zhang Y, Hu S. 2011. Temporal variation of wind speed in China for 1961–2007. *Theor. Appl. Climatol.* **104**: 313–324.

Guo H, Xu M, Hu Q. 2011. Changes in near-surface wind speed in China: 1969–2005. *Int. J. Climatol.* **31**: 349–358.

Jiang Y, Luo Y, Zhao Z, Tao S. 2010a. Changes in wind speed over China during 1956–2004. *Theor. Appl. Climatol.* **99**: 421–430.

Jiang Y, Luo Y, Zhao Z, Shi Y, Xu Y, Zhu J. 2010b. Projections of wind changes for 21st century in China by three regional climate models. *Chin. Geogr. Sci.* **20**: 226–235.

Jiang Y, Luo Y, Zhao Z. 2010c. Projection of wind speed changes in China in the 21st century by climate models. *Chin. J. Atmos. Sci.* **34**: 323–336 (in Chinese).

Jiang Y, Luo Y, Zhao Z. 2013. Maximum wind speed changes over China. *Acta Meteorol. Sin.* **27**: 63–74.

Kurosaki Y, Shinoda M, Sokolik I, Mikami M. 2009. *Inter-Annual Variation of Threshold Wind Speed for Dust Emission in Mongolia*. EGU General Assembly: Vienna.

Li T. 2010. Monsoon climate variabilities. In *Climate Dynamics: Why Does Climate Vary?*, Sun D-Z, Bryan F (eds). The American Geophysical Union: Washington, DC, 27–51.

Li JP, Zeng QC. 2002. A unified monsoon index. *Geophys. Res. Lett.* **29**: 1274, doi: 10.1029/2001GL013874.

Li JP, Zeng QC. 2003. A new monsoon index and the geographical distribution of the global monsoons. *Adv. Atmos. Sci.* **20**: 299–302.

Li Y, Wang Y, Chu H, Tang J. 2008. The climate influence of anthropogenic land-use changes on near-surface wind energy potential in China. *Chin. Sci. Bull.* **53**: 2859–2866.

Li X, Zhong S, Bian X, Heilman WE. 2010. Climate and climate variability of the wind power resources in the Great Lakes region of the United States. *J. Geophy. Res.* **115**: D18107, doi: 10.1029/2009JD013415.

Liao S, Liu K, Li Z. 2008. Estimation of grid based spatial distribution of wind energy resources in China. *Geogr. Inf. Sci.* **10**: 551–556. (in Chinese).

Lin C, Yang K, Qin J, Fu R. 2013. Observed coherent trends of surface and upper-air wind speed over China since 1960. *J. Clim.* **26**: 2891–2903.

Lu X, McElroy MB, Kiviluoma J. 2009. Global potential for wind-generated electricity. *Proc. Natl. Acad. Sci. U. S. A.* **106**: 10933–10938.

Madhu S, Payal S. 2014. A review of wind energy scenario in India. *Int. Res. J. Environ. Sci.* **3**: 87–92.

Mann HB. 1945. Nonparametric tests against trend. *Econometrica* **13**: 245–259, doi: 10.2307/1907187.

Mantua NJ, Hare SR, Zhang Y, Wallace JM, Francis RC. 1997. A Pacific interdecadal climate oscillation with impacts on salmon production. *Bull. Am. Meteorol. Soc.* **78**: 1069–1079.

McElroy MB, Lu X, Nielsen CP, Wang Y. 2009. Potential for wind-generated electricity in China. *Science* **325**: 1378–1380.

McVicar TR, Van Niel TG, Li ML, Roderick ML, Rayner DP, Ricciardulli L, Donohue RJ. 2008. Wind speed climatology and trends for Australia, 1975–2008: capturing the stilling phenomenon and comparison with near-surface reanalysis output. *Geophys. Res. Lett.* **35**: L20403, doi: 10.1029/2008GL035627.

Niu F, Li Z, Li C, Lee K-H, Wang M. 2010. Increase of wintertime fog in China: potential impacts of weakening of the Eastern Asian monsoon circulation and increasing aerosol loading. *J. Geophys. Res.* **115**: D00K20, doi: 10.1029/2009JD013484.

Pimenta F, Kempton W, Garvine R. 2008. Combining meteorological stations and satellite data to evaluate the offshore wind power resource of Southeastern Brazil. *Renew. Energy* **33**: 2375–2387.

Pryor SC, Barthelmie RJ. 2011. Assessing climate change impacts on the near-term stability of the wind energy resources over the United States. *Proc. Natl. Acad. Sci. U.S.A.* **108**(20): 8167–8171, doi: 10.1073/pnas.1019388108.

Rahim NAA, Juneng L, Tangang FT. 2013. Wind-wave simulation in South China Sea: preliminary results of model evaluation using different wind forcing. In *Proceedings of the University Kebangsaan Malaysis*, Selangor, Malaysia.

Saha S, Moorthi S, Pan H-L, Wu X, Wang J, Nadiga S, Tripp P, Kistler R, Woollen J, Behringer D, Liu H, Stokes D, Grumbine R, Cayno G, Wang J, Hou Y-T, Chuang H-Y, Juang H-MH, Sela J, Iredell M, Treadon R, Kleist D, Delst PV, Keyser D, Derber J, Ek M, Meng J, Wei H, Yang R, Lord S, Dool HVD, Kumar A, Wang W, Long C, Chelliah M, Xue Y, Huang B, Schemm J-K, Ebisuzaki W, Liu R, Xie P, Chen M, Zhou S, Higgins W, Zou C-Z, Liu Q, Chen Y, Han Y, Cucurull L, Reynolds RW, Rutledge G, Goldberg M. 2010. The NCEP Climate Forecast System Reanalysis. *Bull. Am. Meteorol. Soc.* **91**: 1015–1057.

Saha S, Moorthi S, Wu X, Wang J, Nadiga S, Tripp P, Behringer D, Hou Y-T, Chuang H-Y, Iredell M, Ek M, Meng J, Yang R, Mendez MP, Dool HVD, Zhang Q, Chen M, Becker E. 2014. The NCEP climate forecast system version 2. *J. Clim.* **27**: 2185–2208.

Schiemann R, Lüthi D, Schär C. 2009. Seasonality and interannual variability of the westerly jet in the Tibetan Plateau region. *J. Clim.* **22**: 2940–2957.

Wang Z, Ding Y, He J, Yu J. 2004. An updating analysis of the climate change in China in recent 50 years. *Acta Meteorol. Sin.* **62**: 228–236. (in Chinese).

Xu M, Chang C-P, Fu C, Qi Y, Robock A, Robinson D, Zhang H. 2006. Steady decline of east Asian monsoon winds, 1969–2000: evidence from direct ground measurements of wind speed. *J. Geophys. Res.* **111**: D24111, doi: 10.1029/2006JD007337.

Yu L, Zhong S, Bian X, Heilman W. 2014. Temporal and spatial variability of wind resources in the United Sates as derived from the Climate Forecast System Reanalysis. *J. Clim.* **28**: 1166–1183, doi: 10.1175/JCLI-D-14-00322.1.

Zhang Y, Sperber KR, Boyle JS. 1997. Climatology and interannual variation of the East Asian winter monsoon: results from the 1979–1995 NCEP/NCAR reanalysis. *Mon. Weather Rev.* **125**: 2605–2619.

Zheng CW, Pan J. 2014. Assessment of the global ocean wind energy resource. *Renew. Sustain. Energy Rev.* **33**: 382–391.

Zheng CW, Pan J, Li J. 2013. Assessing the China Sea wind energy and wave energy resources from 1988 to 2009. *Ocean Eng.* **65**: 39–48.

Zhou W, Yang H, Fang Z. 2006. Wind power potential and characteristic analysis of the Pearl River Delta region, China. *Renew. Energy* **31**: 739–753.

Zuo H, Li D, Hu Y, Bao Y, Lu S. 2005. Characteristics of climatic trends and correlation between pan-evaporation and environmental factors in the last 40 years over China. *Chin. Sci. Bull.* **50**: 1235–1241.

